On Clutter Rank Observed by Arbitrary Arrays

Nathan A. Goodman, *Member, IEEE*, and James M. Stiles, *Senior Member, IEEE*

***Abstract*—This paper analyzes the rank and eigenspectrum of the clutter covariance matrix observed by space-time radar systems with arbitrarily configured arrays and varying look geometry. Motivated by recent applications that suggest use of nonuniform antenna arrays, a generalized theory of clutter rank is derived and demonstrated. First, a one-dimensional effective random process is defined by projecting the measurements obtained by an arbitrary space-time radar system into an equivalent one-dimensional sampling structure. Then, this projection and the Karhunen–Loeve representation of random processes are used to predict clutter rank based on effective aperture-bandwidth product. Simulated results are used to confirm the theory over a wide range of scenarios, and along the way, the well-known Brennan's rule for clutter rank is shown to be a special case of the proposed aperture-bandwidth product.**

***Index Terms*—Adaptive radar, radar clutter, radar signal processing.**

I. Introduction

In recent years, the implementation of space-time adaptive processing (STAP) on platforms that employ nonuniform or nonlinear arrays has become increasingly prevalent. Circular, conformal, and distributed array geometries [1]–[5] have all been considered as possible antenna configurations for STAP. The goals of these geometries include enabling 360-degree coverage, avoiding degradation of platform aerodynamics, and/or implementing wide spatial baselines that improve minimum detectable velocity (MDV).

The matrix that quantifies the correlation between all pairs of space-time measurements due to reflections from ground clutter is called the clutter covariance matrix (CCM). The rank of the CCM (termed *clutter rank*) affects the amount of data required to train an adaptive processor as well as the overall detection performance of the system. Accurate clutter rank estimation is important for the design of computationally feasible, reduced-order adaptive processing algorithms. Therefore, characterization of clutter rank is an important step for understanding STAP performance. Clutter rank is well understood for uniform, linear arrays aligned along the radar platform's velocity vector and when the system's pulse repetition frequency (PRF) is matched to the antenna element spacing. The equation that governs this case is called Brennan's rule [6], [7]. The clutter rank observed by arbitrary arrays, however, is less well understood.

Manuscript received September 6, 2005; revised January 5, 2006. The associate editor coordinating the review of this manuscript and approving it for publication was Dr. Marelo G. S. Bruno.

N. A. Goodman is with the Department of Electrical and Computer Engineering, University of Arizona, Tucson, AZ 85721-0104 USA (e-mail: goodman@ece.arizona.edu).

J. M. Stiles is with the Radar Systems and Remote Sensing Laboratory, University of Kansas, Lawrence, KS 66045 USA (e-mail: jstiles@eecs.ku.edu).

Digital Object Identifier 10.1109/TSP.2006.882071

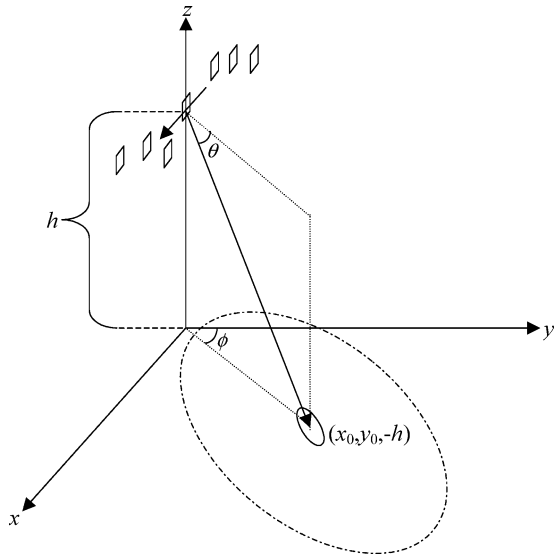

Fig. 1. Radar system geometry.

In this paper, a generalization of Brennan's rule is derived using the Karhunen–Loeve (KL) representation of random processes. First, the space-time clutter measurements are projected into a one-dimensional sampling structure yielding an effective one-dimensional random process. Then, we apply the KL expansion in the limit as the observation interval becomes large in order to predict the numerical rank of the CCM. The rank depends on the power spectral density (PSD) of the equivalent one-dimensional random process and on the overall observation window of the equivalent one-dimensional sampling structure.

In Section II, we present the radar model and geometry used in this paper. We also present the space-time measurement projection mentioned above. In Section III, we discuss the KL foundation for clutter rank and use that foundation to derive a generalized expression for clutter rank. We also show that the generalized expression reduces to Brennan's rule in the special case of a uniform, linear array aligned along the radar platform's velocity vector. In Section IV, we show simulated results that confirm our analysis. Last, we make our conclusions in Section V.

II. Radar Model and Measurement Projection

A. Signal and Clutter Covariance Model

The assumed radar geometry, shown in Fig. 1, uses the same conventions as in [7]. The radar system travels in the positive x-direction at velocity, v, and the array phase reference at time zero is located at the origin of the coordinate system. Therefore, assuming a flat Earth, the z-coordinate of all points on the ground is $-h$, where h is the altitude of the array phase reference. The elevation angle is θ, and the azimuth angle is ϕ. The antenna array is made up of arbitrarily located antenna elements

all moving with the same x-directed velocity. The narrowband approximation is assumed, which forces the range bins of each spatial channel to be aligned and is consistent with parameters typical of moving target indication (MTI) radar modes. For this paper, the antennas operate coherently on transmit, but all antennas possess their own receivers. Therefore, the gain patterns of the individual elements on receive are much wider than the illumination pattern on transmit.

From Fig. 1, the vector defining the position of a point on the Earth's surface, $\mathbf{x}$, is $\mathbf{x} = [x \;\; y \;\; -h]^\dagger$ where $(\cdot)^\dagger$ denotes the matrix or vector transpose operation. The effective phase center on transmit is taken to be the array phase reference, which passes through the origin at time $t = 0$. The radar system's velocity vector is $\mathbf{v} = [v \; 0 \; 0]^\dagger$, and the location of a receiver at $t = 0$ is defined as $\mathbf{r} = [r_x \; r_y \; r_z]^\dagger$.

The signal received from a point scatterer at position $\mathbf{x}$ is a scaled and delayed version of the transmitted signal. Employing the narrowband assumption in the matched-filtering and down-conversion steps, the complex signal collected by a receiving antenna due to a single stationary scatterer is

$$\tilde{s}_0(\mathbf{x}, \mathbf{r}, t) = \frac{\gamma_0(\mathbf{x}) g(\mathbf{x})}{R_0^2} \exp\left[-j\omega_0 \tau(\mathbf{x}, \mathbf{r}, t)\right] \tag{1}$$

where $g(\mathbf{x})$ is the field intensity pattern of the transmit array, R_0 is the distance to the range bin under consideration, $\tau(\mathbf{x}, \mathbf{r}, t)$ is the two-way propagation delay at time t to the receiver at position $\mathbf{r}$, $\gamma_0(\mathbf{x})$ is the point scatterer's reflection coefficient, and ω_0 is the carrier frequency. While (1) represents the signal received from a single point scatterer, the complete space-time signal is due to all scatterers within a constant range contour. Using R_0 to denote the iso-range contour of interest, the complete received signal is

$$\begin{aligned}\tilde{s}(\mathbf{r}, t) &= \int_{R_0} \tilde{s}_0(\mathbf{x}, \mathbf{r}, t) d\mathbf{x} \\ &= \frac{1}{R_0^2} \int_{R_0} \gamma_0(\mathbf{x}) g(\mathbf{x}) \exp\left[-j\omega_0 \tau(\mathbf{x}, \mathbf{r}, t)\right] d\mathbf{x}. \end{aligned} \tag{2}$$

For simulation purposes, the integration in (2) is approximated. The iso-range contour is divided in the cross-range dimension into cells called clutter patches. Then, letting $\gamma_i = \gamma(\mathbf{x}_i)$ be the effective reflection coefficient for the i^{th} clutter patch, a discrete model for (2) is

$$\tilde{s}(\mathbf{r}, t) \approx \frac{1}{R_0^2} \sum_{i=1}^{N_c} \gamma_i g(\mathbf{x}_i) \exp\left[-j\omega_0 \tau(\mathbf{x}_i, \mathbf{r}, t)\right]. \tag{3}$$

Finally, the radar collects samples of the received waveform at multiples of the pulse repetition interval (PRI) at each antenna element. For M pulses and N antennas, the radar collects MN space-time measurements defined by

$$\tilde{s}(\mathbf{r}_n, t_m) \approx \frac{1}{R_0^2} \sum_{i=1}^{N_c} \gamma_i g(\mathbf{x}_i) \exp\left[-j\omega_0 \tau(\mathbf{x}_i, \mathbf{r}_n, t_m)\right] \tag{4}$$

where $\mathbf{r}_n$ is the position of the n^{th} antenna element relative to the array reference and $t_m = mT_R$ is the instant of the m^{th} time sample. The space-time steering vector, $\mathbf{v}(\mathbf{x}_i)$, is defined by stacking the space-time samples of (4)

$$\begin{aligned}\mathbf{v}(\mathbf{x}_i) = \Big[& e^{-j\omega_0 \tau(\mathbf{x}_i, r_1, t_1)} \; e^{-j\omega_0 \tau(\mathbf{x}_i, r_1, t_2)} \\ & \cdots e^{-j\omega_0 \tau(\mathbf{x}_i, r_1, t_{M-1})} \cdots e^{-j\omega_0 \tau(\mathbf{x}_i, r_{N-1}, t_{M-1})} \Big] \end{aligned} \tag{5}$$

which allows the discrete, measured signal to be represented as

$$\mathbf{s} \approx \frac{1}{R_0^2} \sum_{i=1}^{N_c} \gamma_i g(\mathbf{x}_i) \mathbf{v}(\mathbf{x}_i). \tag{6}$$

Let the γ_i's be modeled as independent, circularly complex Gaussian random variables with variance $\sigma_i^2 = \mathrm{E}[|\gamma_i|^2]$ where $\mathrm{E}[\cdot]$ is the expected value operator. The vector $\mathbf{s}$ is then a multivariate Gaussian random variable with (clutter) covariance matrix defined as

$$\mathbf{K} = \mathrm{E}[\mathbf{s}\mathbf{s}^{\mathrm{H}}] \tag{7}$$

where the superscript H denotes conjugate transpose. Substituting (6) into (7) and employing the independence assumption, the CCM is

$$\mathbf{K} = \frac{1}{R_0^4} \sum_{i=1}^{N_c} \sigma_i^2 g(\mathbf{x}_i)^2 \mathbf{v}_i \mathbf{v}_i^{\mathrm{H}}. \tag{8}$$

Equation (8) will be used to generate the ideal CCMs used to produce the results in Section IV.

B. Space-Time Measurement Projection

The following measurement projection allows clutter to be approximated as a one-dimensional random process for arbitrary, three-dimensional arrays. It also facilitates analysis of nonsidelooking scenarios.

Under the narrowband approximation, measurements taken at different points in space and time can be represented as relative phase shifts that can be expressed as a sum of Doppler and spatial frequencies. Let the phase history of (1) be

$$\begin{aligned} & -\omega_0 \tau(\mathbf{x}, \mathbf{r}, t) \\ & \quad = \Psi(\mathbf{x}, \mathbf{r}, t) \\ & \quad = k_x(\mathbf{x}) r_x + k_y(\mathbf{x}) r_y + k_z(\mathbf{x}) r_z + \omega_D(\mathbf{x}) t. \end{aligned} \tag{9}$$

Then, according to the geometry of Fig. 1, the unit vector pointing from the array reference to the point $\mathbf{x}$ at $t = 0$ is

$$\hat{\mathbf{k}} = \cos\theta \sin\phi \hat{\mathbf{x}} + \cos\theta \cos\phi \hat{\mathbf{y}} - \sin\theta \hat{\mathbf{z}} \tag{10}$$

which leads to the following definitions of the Doppler and spatial frequencies

$$\begin{aligned} \omega_D(\mathbf{x}) &= \frac{2\pi}{\lambda} 2v \cos\theta \sin\phi = \frac{2\pi}{\lambda} \frac{2vx}{R_0} \\ k_x(\mathbf{x}) &= \frac{2\pi}{\lambda} \cos\theta \sin\phi = \frac{2\pi}{\lambda} \frac{x}{R_0} \\ k_y(\mathbf{x}) &= \frac{2\pi}{\lambda} \cos\theta \cos\phi = \frac{2\pi}{\lambda} \frac{y}{R_0} \\ k_z(\mathbf{x}) &= -\frac{2\pi}{\lambda} \sin\theta = -\frac{2\pi}{\lambda} \frac{h}{R_0}. \end{aligned} \tag{11}$$

In order to arrive at the desired projection, we evaluate the first-order Taylor expansion of (9) with the derivative taken in the cross-range direction. Defining $\overline{\mathbf{x}} = [x_0 \;\; y_0 \;\; -h]^\dagger$ as the central point of illumination on the ground and the point around which the expansion is performed, the expansion is

$$\Psi(\mathbf{x},\mathbf{r},t) = \Psi(\mathbf{x},\mathbf{r},t)\big|_{\mathbf{x}=\overline{\mathbf{x}}} + (\nabla_x \Psi)_p\big|_{\mathbf{x}=\overline{\mathbf{x}}}\,\Delta p \quad (12)$$

where

$$\nabla_x = \left[\frac{\partial}{\partial x} \quad \frac{\partial}{\partial y} \quad \frac{\partial}{\partial z}\right]^\dagger \quad (13)$$

is the gradient operator versus scatterer location and $(\nabla_x \Psi)_p$ is the projection of the gradient operator in the cross-range direction. A unit vector in the cross-range direction can be defined as

$$\hat{\mathbf{p}} = \cos\phi\hat{\mathbf{x}} - \sin\phi\hat{\mathbf{y}} + 0\hat{\mathbf{z}} \quad (14)$$

which leads to

$$\begin{aligned}(\nabla_x \Psi)_p &= \nabla_x \Psi \cdot \hat{\mathbf{p}} \\ \Delta p &= \boldsymbol{\Delta x} \cdot \hat{\mathbf{p}} = (x - x_0)\cos\phi - (y - y_0)\sin\phi. \end{aligned} \quad (15)$$

Combining (11)–(15) yields the following expression for the second term of (12)

$$\begin{aligned}(\nabla_x \Psi)_p\big|_{\mathbf{x}=\overline{\mathbf{x}}}\,\Delta p = \frac{2\pi}{\lambda}\frac{(x - x_0)\cos\phi - (y - y_0)\sin\phi}{R_0} \\ \times\left[(r_x + 2vt)\cos\phi - r_y \sin\phi\right]. \end{aligned} \quad (16)$$

Equation (16) represents the received phase history in the projected coordinate system. Hence, a new spatial frequency can be defined as

$$k_\alpha(\mathbf{x}) = \frac{2\pi}{\lambda}\frac{(x - x_0)\cos\phi - (y - y_0)\sin\phi}{R_0} \quad (17)$$

a new sampling coordinate system as

$$r_\alpha(r_x, r_y, t) = (r_x + 2vt)\cos\phi - r_y \sin\phi \quad (18)$$

and an approximate phase history of

$$\Psi(\mathbf{x},\mathbf{r},t) = k_\alpha(\mathbf{x}) r_\alpha(r_x, r_y, t). \quad (19)$$

Clutter can now be treated as an effective one-dimensional random process. The power spectral density of the effective random process is obtained by projecting the average received power versus position $\mathbf{x}$ into a function of average power versus $k_\alpha(\mathbf{x})$. The new random process is sampled in one dimension at locations obtained by projecting the original space-time sample locations into the new coordinate system [8]. These two projections are defined by (17) and (18), respectively. As with any Taylor expansion of a function, the resulting expression loses accuracy when it is evaluated away from the original expansion point. For our application, this implies that the expanded phase history in (12) or (19) is most accurate for points near the center of the illumination beam. For processing techniques based on (19), one should carefully consider the validity of the first-order Taylor expansion over the range of radar parameters for the current application. For the analysis in this paper, however, the related projections in (17) and (18) are used to find an effective aperture and spectral clutter profile. The accuracy of the first-order expansion seems to have little or no effect on the results of Section IV. Furthermore, an analogy can be made between the first-order projection presented here and other common first-order approximations such as ignoring range or Doppler walk. These approximations often allow efficient, accurate characterization of a basic system even if they cannot be applied in a final processing algorithm.

A comment should also be made concerning the fact that we have dropped the first term of (12) in the new representation. This term is evaluated at the expansion point of the Taylor series. Hence, if the expansion point is chosen near the center of the illumination beam, the first term contains the center spatial and Doppler frequencies. For a sidelooking geometry, for example, the Doppler shifts returning from the illuminated area are centered around zero Doppler. If, however, the illumination pattern is scanned ahead of sidelooking, then the center Doppler frequency is positive. When the first term of (12) is present, the one-dimensional random process may be viewed as a bandpass process with center frequency defined by that first term. By ignoring this center-frequency term, we have derived an equivalent baseband representation.

III. Clutter Rank

Clutter rank characterizes the severity of ground clutter. High clutter rank relative to the measurement dimension implies that most measurement dimensions are required for representation of the clutter, leaving few clutter-free dimensions available for moving target detection. On the other hand, low clutter rank relative to the measurement dimension implies that there are many dimensions available for moving target detection. Consider the problem in the following way. If the radar collects MN independent measurements, then moving targets can exist anywhere in MN-dimensional space. In some of that space, moving targets compete with ground clutter. However, we have not yet characterized how much of the MN-dimensional space is occupied by clutter, or how powerful the clutter is in those regions. How do we know if there will be a low-clutter region of the measurement space, and if so, how large will that region be? These questions are answered by understanding the rank and eigenspectrum of the clutter covariance matrix, and the answers to these questions help to determine MTI performance. Although expressions for clutter rank exist for specific situations, a general description of clutter rank for different look geometries and array configurations is still needed.

A. Brennan's Rule

There is one particular set of assumptions where clutter rank is well understood. If the array elements are aligned along the velocity vector of the radar and spaced uniformly such that spatial Nyquist sampling is just achieved, and if the PRF is chosen such that the spacing coefficient, $\beta = 2vT_R/d$ [7], is an integer, then clutter rank, r_c, follows Brennan's rule [6], [7]:

$$r_c = N + (M - 1)\beta \quad (20)$$

where N is the number of array elements and M is the number of transmitted pulses. Equation (20) is proved by counting the number of unique measurements obtained by the radar [7]. Because β is an integer, some measurements are repeated, and it is trivial to count the number of unique measurements. Unique measurements contribute nonzero eigenvalues to the CCM while redundant measurements each contribute a zero eigenvalue. Therefore, if the eigenvalues of the CCM are plotted in decreasing order, there is a sharp transition between nonzero and zero eigenvalues that can be interpreted as the rank of the CCM. Unfortunately, the assumptions necessary for Brennan's rule to be strictly valid do not usually apply in practice although it has been shown in [7] that Brennan's rule can be approximately correct when the assumptions are relaxed. Klemm [9]–[12] has also studied clutter rank under similar conditions.

B. The Synthetic Aperture-Bandwidth Product

While Brennan's rule is useful for estimating clutter severity for sidelooking scenarios, a more general clutter characterization is desirable. Sidelooking scenarios are not the only scenarios of interest, and the *unique-measurement* approach that is the foundation of Brennan's rule is not applicable to arbitrarily configured arrays.

In [13], the number of unique signals observed by an array over multiple pulses was shown to depend on the spatial bandwidth of the signals impinging on the array and the total observation time from the arrival of the first pulse at the first array element to the arrival of the last pulse at the last element. In other words, the rank of the measurements depended on the observed time-bandwidth product, which is known as the Landau–Pollak theorem [14]. In fact, Brennan's rule can be obtained from the time-bandwidth product for the special case of Nyquist spatial sampling [15]. For element spacing, d, and full azimuth illumination, the spatial bandwidth, B_s, is $1/d$. The length of the synthetic aperture, L_s, created by the moving array is $(N-1)d+2v(M-1)T_R$ (the factor of two comes from the fact that both the transmitting and receiving phase center move, yielding an effective motion that is twice the real motion). Applying the spatial bandwidth and the synthetic aperture to the Landau–Pollak theorem yields

$$\begin{aligned} r_c &= L_s B_s + 1 = \left[(N-1)d + 2v(M-1)T_R\right]\frac{1}{d} + 1 \\ &= N + (M-1)\frac{2vT_R}{d}. \end{aligned} \tag{21}$$

Recognizing the usual definition of β yields Brennan's rule. Therefore, Brennan's rule is a form of the received time-bandwidth product, which for Nyquist spatial sampling and integer β also happens to be the number of unique measurements collected.

Here, we generalize clutter rank using the KL expansion of a random process. The KL expansion represents a random process with a weighted sum of orthonormal functions with uncorrelated coefficients. The orthonormal functions are the solutions to the integral equation

$$\lambda_j \psi_j(t) = \int_0^L K_s(t,u)\psi_j(u)du \tag{22}$$

where the λ_j's and $\psi_j(t)$'s are the eigenvalues and eigenfunctions of (22) and $K_s(t,u)$ is the covariance function of the random process $s(t)$. Two interesting properties of the eigenvalues and eigenfunctions of the KL expansion will be exploited [16], [17]. First, when a stationary, bandlimited (bandwidth B) random process is observed over a finite aperture L, there are approximately $(BL+1)$ significant eigenvalues. Second, when the random process is stationary and the observation aperture L is large, the eigenfunctions become evenly spaced sinusoids with corresponding eigenvalues proportional to the process' PSD at that frequency. Each time-limited sinusoidal eigenfunction has an approximate bandwidth of $\Delta f = 1/L$. It is then easy to see that it takes $(BL+1)$ sinusoids of width $1/L$ to span the bandwidth B.

This asymptotic relationship between the eigenvalues, eigenfunctions, and PSD of the random process allow a more precise definition of clutter rank. Let clutter rank be defined as the number of eigenfunctions necessary to represent a fraction, ε_P, of the total received clutter power. Thus, ε_P is defined as

$$\varepsilon_P = \frac{P_{B_{sub}}}{P} = \frac{\int_{B_{sub}} |G_s(f)|\,df}{\int_{-\infty}^{\infty} |G_s(f)|\,df} \tag{23}$$

where $G_s(f)$ is the PSD of the random process, P_{Bsub} is the average clutter power within the subband B_{sub}, and P is the total average clutter power. The number of eigenfunctions, r_c, necessary to span the subband is the aperture-bandwidth product plus one

$$r_c = B_{sub}L + 1 \tag{24}$$

where L is the length of the observation interval over which the clutter random process must be represented and the interval over which the eigenfunctions are defined. Using (23), the average power within a specified bandwidth can also be written as a summation of the first r_c eigenvalues of the CCM

$$P_{B_{sub}} = \Delta f \sum_{i=1}^{r_c} \lambda_i. \tag{25}$$

If, for example, we desire to define clutter rank as the number of measurement dimensions necessary to represent 95 percent of the expected clutter power, the clutter PSD and (23) can be used to determine the required subband bandwidth, B_{sub}. Then, the length of the observing interval and (24) can be used to find the required number of dimensions.

The measurement project of Section II is required in order to apply the aperture-bandwidth product to arbitrary array configurations and nonsidelooking configurations. In these cases, an effective PSD is obtained by projecting the cross-range clutter power profile onto the frequency axis k_α. Likewise, the observation aperture is obtained by projecting the original space-time measurement locations into the effective coordinate axis α. Examples of this procedure are presented in Section IV.

C. Sampling Effects

The aperture-bandwidth product defined above applies to a continuous observation window or aperture, but the STAP signal

model describes data sampled in space and time. Some of the effects of sampling in space and time are discussed in the following. The discussion is separated into two cases: periodic sampling and nonperiodic sampling. When the effective sampling structure is periodic, spectral aliasing can occur. When the structure is nonperiodic, aliasing does not occur, but the sampling density affects the clutter analysis.

1) Periodic Sampling: Periodic sampling occurs when projection of the physical space-time sample locations onto the effective coordinate system results in uniformly spaced samples. For example, when spatial samples are separated along the radar velocity vector with inter-element spacing equal to half the distance traveled by the radar during a PRI, the DPCA ($\beta = 1$) condition occurs. In this case, some samples overlap precisely and can be considered as a single effective sample. In general, periodic sampling occurs most often when uniformly spaced antennas are aligned along the direction of travel and either β or $1/\beta$ is an integer; however, other situations can lead to periodic sampling as well.

Because of the uniform sampling interval, aliasing can occur when the effective illuminated bandwidth is larger than the effective sampling rate. Let B_α be the bandwidth of the clutter random process in the effective coordinate system. Aliasing occurs when $B_\alpha > 1/d_\alpha \triangleq F_\alpha$. Whether aliasing is present or not, the aperture-bandwidth product applies, but the maximum bandwidth that can be used in the aperture-bandwidth product is F_α. When aliasing is present, the clutter eigenvalues will take on values of the aliased PSD rather than the true PSD. That is, the clutter PSD that must be used in (23) is obtained by folding the unaliased PSD into the range $[-F_\alpha/2, F_\alpha/2)$.

2) Nonperiodic Sampling: Nonperiodic sampling occurs when the projected samples are not uniformly spaced, such as might occur for arbitrarily configured arrays. To facilitate this discussion, let the average distance between samples in the effective coordinate system be denoted by $\overline{d}_\alpha = L_\alpha/MN$, the average sampling rate be $\overline{F}_\alpha = 1/\overline{d}_\alpha$, and the number of measurements be MN. Several cases of different sampling density are considered in the following.

First, consider the case where $\overline{F}_\alpha/B_\alpha \geq 1$. In this case, the average sampling rate satisfies the Nyquist rate, and the synthetic-aperture analysis can be applied directly. In the results shown in Section IV, it will be observed that the synthetic-aperture analysis seems to be most accurate for $\overline{F}_\alpha/B_\alpha \gg 1$. In this situation, the analysis is very accurate because the average sampling rate easily exceeds the Nyquist rate, resulting in well-defined sinusoidal eigenfunctions that accurately represent the random process. For cases where the average sampling rate barely exceeds the Nyquist rate, the eigenvalues follow the PSD less closely because the sampling is less dense and the sinusoidal eigenfunctions are less well defined.

Next, consider the case where $\overline{F}_\alpha/B_\alpha < 1$. This can occur when either the effective temporal sampling is much larger than the effective array size or when the effective spatial sampling is much larger than the synthetic aperture of individual antennas. The second possibility, known as the distributed-array case, is more likely and implies that the clutter measurements collected by different antennas are uncorrelated due to their large separation. The CCM then becomes a block-diagonal matrix, and the eigenvalues of the CCM are the eigenvalues of the individual blocks. Therefore, the clutter rank of the full system is equal to the sum of the temporal clutter ranks for the individual antennas. Furthermore, since the effective temporal sampling will be the same for each antenna, the eigenvalues of each block in the CCM are identical. If r'_c is the clutter rank due to a single antenna, then the overall system clutter rank will be Nr'_c.

For distributed arrays, since the data samples from adjacent antennas do not overlap, there are no opportunities for forcing redundant measurements in this situation, and clutter energy will fill all dimensions of the measurement space unless the effective clutter bandwidth is severely limited by a very narrow transmit pattern. Hence, space-time filtering is unlikely to yield much benefit in this situation.

TABLE I
STAP SIMULATION PARAMETERS

Parameter	Value
Altitude	10 km
Elevation Angle	5°
Radar Velocity	200 m/s
Carrier Frequency	450 MHz
PRF	300 Hz
Number of Pulses	128
Number of Antennas	5

IV. RESULTS

The results in this section compare the eigenvalues of the ideal CCM to the PSD underlying the random process. The power represented by the eigenvalues is also compared to the theoretical power within a specified bandwidth obtained by integrating the PSD. Sidelooking, periodically sampled systems are considered first. Then, nonperiodic systems are evaluated followed by two nonsidelooking simulations. The distributed-aperture case is considered last.

A standard three-dimensional STAP simulation was developed. The simulation divides a constant range ring into many clutter patches. The spatial and Doppler frequencies of each patch are determined, and the space-time steering vectors are computed using (5) and (9). The ground was assumed to be homogeneous within the range bin under consideration; therefore, the shape of the clutter power density as a function of cross-range was controlled by the transmit illumination pattern [see (8)], which for this analysis was assumed to be in the shape of a hanning function. The width of the transmit pattern was varied in order to implement varying illumination bandwidth. An illumination pattern with sidelobes can also be used if the power fraction in (23) is computed over a disjoint frequency band in order to represent the most clutter power possible within the allocated subband. Additional simulation parameters are provided in Table I. In the following figures, theoretical curves were generated via the aperture-bandwidth theory proposed in this paper

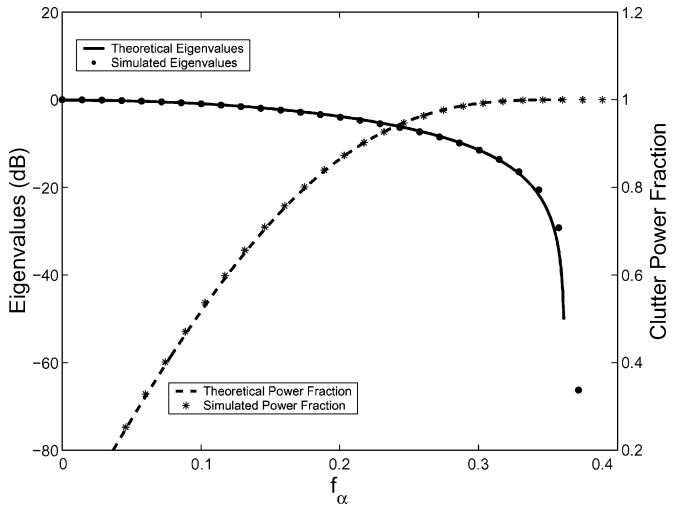

Fig. 2. Theoretical and simulated clutter eigenvalues for sidelooking, periodic case.

while simulated curves refer to results obtained by simulating the ideal CCM of (8).

Results from the first simulation are shown in Fig. 2. For this simulation, the antennas were place in a uniform, linear array aligned with the radar velocity vector. The antenna spacing was matched to the radar PRF such that $\beta = 1$. The transmit illumination was focused in a sidelooking configuration with an absolute beamwidth spanning $\pm 14^\circ$. With this beamwidth and the parameters in Table I, no aliasing occurs. The descending plots in Fig. 2 compare the single-sided PSD and the eigenvalues of the CCM. It is seen that the eigenvalues follow the PSD curve very closely. The ascending curve with scale shown on the right side of the graph show the average power within a specified bandwidth as well as the power contained within the first $2L_\alpha B_\alpha + 1$ eigenvalues where B_α is defined in this case as a baseband bandwidth from zero to the value shown on the horizontal axis. The factor of two is present because the PSD is symmetric; hence, each eigenfunction represents energy from both sides of the PSD with separation between sinusoids equal to $0.5/L_\alpha$. In this and subsequent figures, only every fifth data point is displayed on the simulated curves to improve clarity.

As an example, the 95-percent point on the power fraction curve of Fig. 2 corresponds to $f_\alpha \approx 0.25$. Hence, 95 percent of the clutter power is contained within the two-sided bandwidth $2f_\alpha = 0.5$. For a sidelooking, uniform linear array with $\beta = 1$, the effective observation aperture is $L_\alpha = 2v(M-1)T_r + (N-1)d = 174.67$, and the aperture bandwidth product is $r_c = 2f_\alpha L_\alpha + 1 = 88.33 \approx 88$. Note that Brennan's rule predicts $r_c = M + (N-1)\beta = 132$. The reason for the difference is that we have applied the aperture-bandwidth product to predict the clutter dimension necessary for representing 95% of the clutter power rather than 100%. If the full clutter bandwidth of $2f_\alpha \approx 0.75$ is used, then the aperture-bandwidth product also predicts $r_c = 132$.

Fig. 3(a) shows the results when aliasing is introduced by increasing the illumination beamwidth to $\pm 22^\circ$. The eigenspectrum exhibits a sharp cutoff at the folding frequency

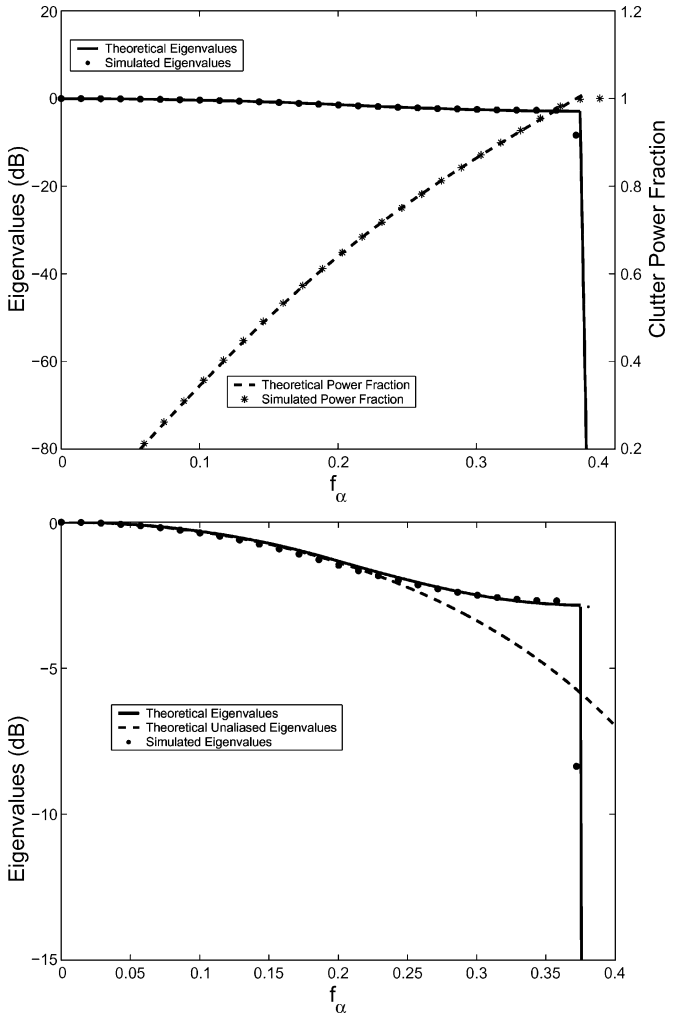

Fig. 3. (a) Theoretical and simulated clutter eigenvalues for sidelooking, periodic case with aliasing. (b) Close-up of the eigenvalues in Fig. 3(a).

corresponding to the uniform sampling interval. The eigenspectrum follows the aliased PSD, which is shown more clearly by the close-up of Fig. 3(b). The aliased PSD is flatter than the unaliased PSD due to the spectral tails that fold back into the spectrum.

Next, we consider the case of nonuniform sampling obtained by randomly perturbing the average antenna locations in the x-, y-, and z-directions. For this geometry, the effective observation aperture is obtained using the data projection of (18). Fig. 4 shows results for a sidelooking case where the average antenna spacing in the along-track direction is equal to twice the distance traveled by the radar in a single PRI. Hence, it can be said that the average β value, $\overline{\beta}$, is equal to unity. The absolute beamwidth has again been set to $\pm 14^\circ$. This is the densely sampled case of nonuniform sampling and leads again to good agreement between the theoretical and simulated eigenvalues. In fact, the plot is nearly identical to Fig. 2, which again confirms the previous assertion that Brennan's rule is equivalent to the aperture-bandwidth product when the underlying sampling satisfies the Nyquist rate.

Fig. 5 shows results when the average along-track antenna spacing is increased such that $\overline{\beta} = 0.01$. Despite the increased

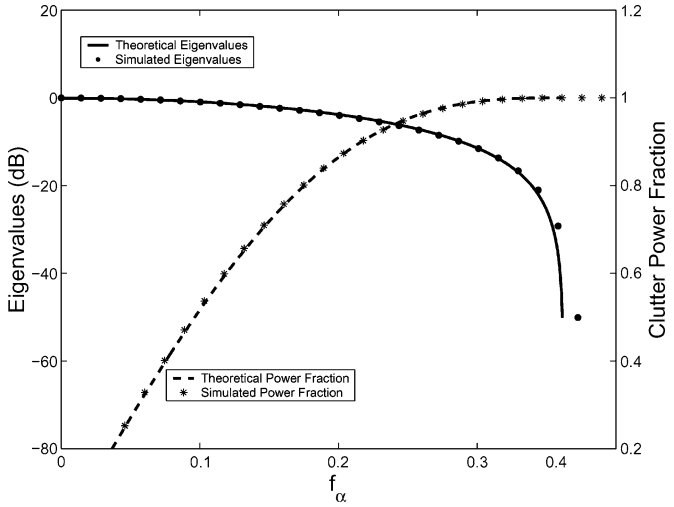

Fig. 4. Theoretical and simulated clutter eigenvalues for sidelooking, nonperiodic case.

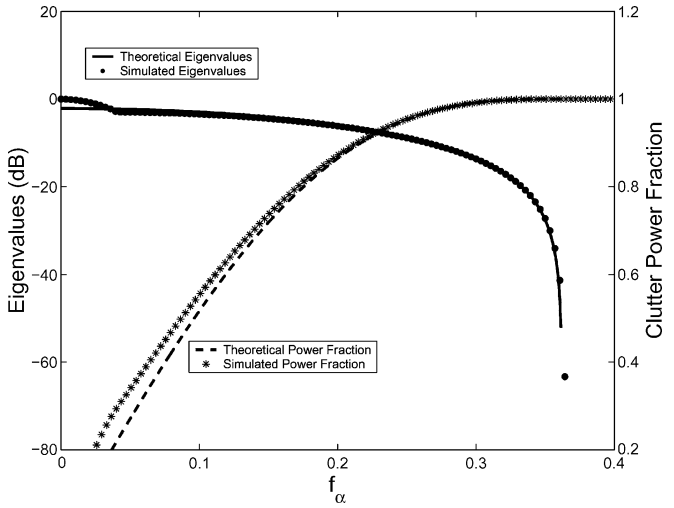

Fig. 5. Theoretical and simulated clutter eigenvalues for sidelooking, nonperiodic case with increased antenna spacing.

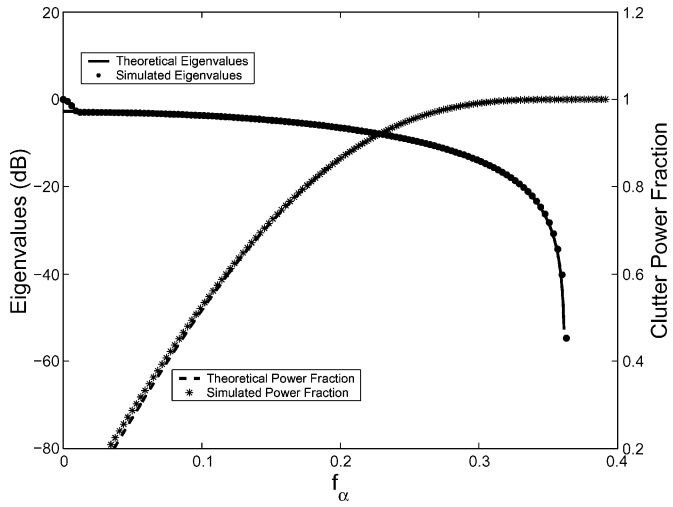

Fig. 6. Theoretical and simulated clutter eigenvalues for sidelooking, nonperiodic case with antenna spacing on the order of the length of a temporal synthetic aperture.

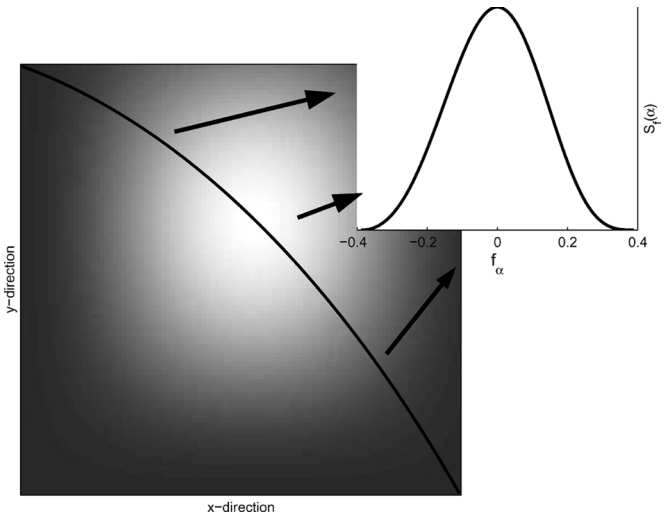

Fig. 7. Visualization of the clutter PSD projection.

spacing, the average sampling rate is still greater than the illuminated bandwidth by a factor of about 1.25. However, there is much less overlap between the effective samples of adjacent antennas, which creates some discrepancy between the largest predicted and simulated eigenvalues. Also, note the increased number of simulated data points in Fig. 5 compared to Figs. 2 and 4. This occurs because the increased antenna spacing has increased the length of the effective aperture. The increased aperture increases the aperture-bandwidth product, which, in turn, requires more eigenfunctions than before to span the same bandwidth.

When the average antenna separation in the along-track direction is further increased such that $\overline{\beta} = 0.008$ and the average sampling rate is approximately 1.1 times the illuminated bandwidth, the theoretical and simulated curves actually seem to converge again. This result, shown in Fig. 6, is apparently due to the fact that the samples from adjacent antennas overlap by only a small amount. Hence, the effective sampling structure has long intervals of uniform sampling determined by the constant PRI. When the samples transition from those of one antenna to another, there is a single nonuniform shift due to the random antenna spacing, followed by another long interval of uniform sampling. The result is a long observing aperture with a quasi-uniform sampling structure that satisfies the Nyquist rate; consequently, the eigenfunctions are well-defined sinusoids and the proposed theory is accurate. The proposed theory seems to be least accurate for moderate antenna spacing where the synthetic apertures of adjacent antennas overlap enough to make the sampling structure appear nonuniform but not enough to make the effective sampling rate much larger than the illuminated bandwidth. Note also that the number of data points in the simulated curves have again increased due to the increased number of eigenfunctions needed to span the specified clutter bandwidth.

Next, we evaluate two forward-looking scenarios since the data projection derived in Section II was partly motivated by its ability to handle nonsidelooking configurations. Fig. 7 shows a two-dimensional hanning transmit pattern and an iso-range

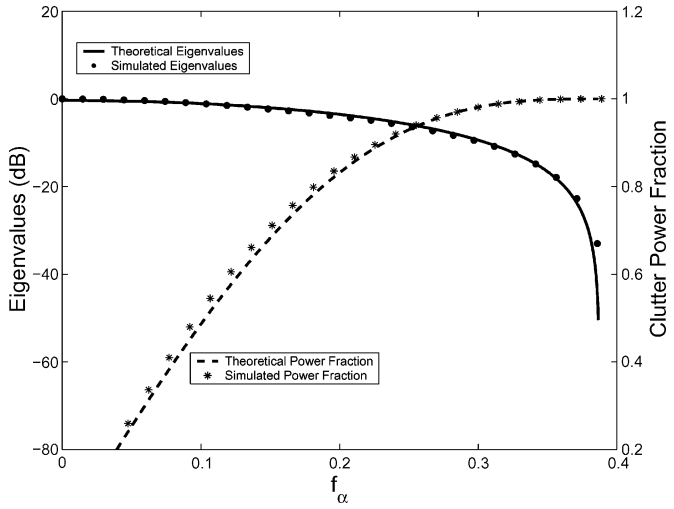

Fig. 8. Theoretical and simulated clutter eigenvalues for forward-looking, nonperiodic case.

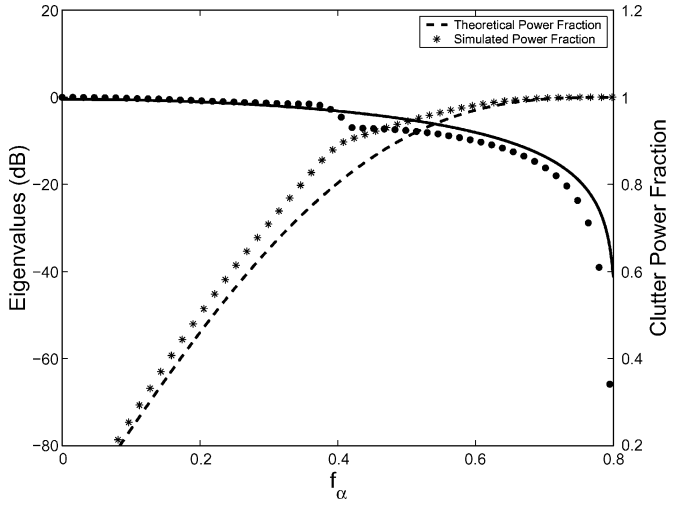

Fig. 9. Theoretical and simulated clutter eigenvalues for forward-looking, nonperiodic case with increased antenna spacing.

contour that cuts through the peak of the pattern. The subplot shows the effective one-dimensional PSD that results from projecting the cross-range power profile into the effective coordinate system. While it is obvious that the structure of the resulting PSD is simply the transmit pattern along the iso-range contour, the projection of (17) properly scales the frequency axis such that it agrees with the units of the projected sampling structure.

When the scenario depicted by Fig. 7 is analyzed, the resulting eigenspectrum is shown in Fig. 8. The theoretical and simulated curves agree very well and resemble the corresponding sidelooking case shown in Fig. 4. When the antenna beamwidth is widened in the forward-looking case such that the ratio of average sampling rate to illuminated bandwidth is approximately 2.5, the results are shown in Fig. 9. The results in Fig. 9 are not as accurate as in Fig. 8, which is reminiscent of how the results of Fig. 5 were not as accurate as the results in Fig. 4. In both Figs. 8 and 9, the average antenna spacing in the along-track direction was such that $\overline{\beta} = 0.267$.

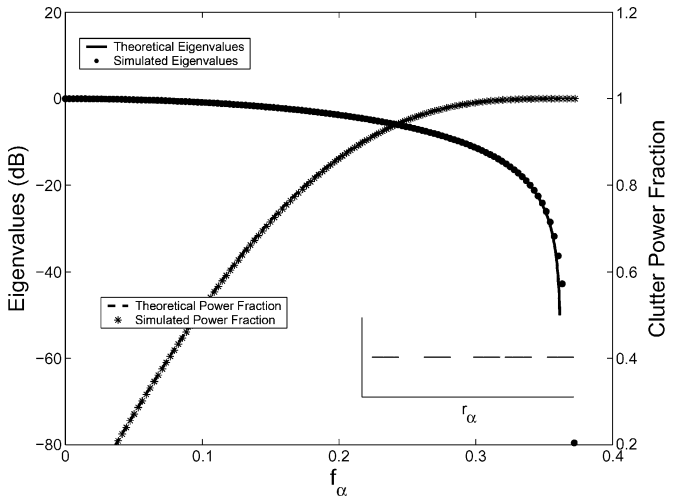

Fig. 10. Theoretical and simulated clutter eigenvalues for sidelooking, nonperiodic, distributed-array case.

The aperture-bandwidth analysis of clutter rank has been shown to be accurate for periodic and nonperiodic sampling and for sidelooking and nonsidelooking configurations. Next, we consider cases of large antenna separation that cause the overall effective sampling rate to be less than the illuminated bandwidth. When this occurs, the effective sampling structure can have large gaps without any space-time samples. These gaps, in turn, can cause the effective aperture length to be overestimated. Fig. 10 shows the eigenspectrum results for the distributed-array scenario. The inset in Fig. 10 depicts the effective sampling structure of the distributed, arbitrary-array system and shows the five distinct regions of sampling corresponding to the synthetic apertures of individual antennas. The gaps in the sampling structure show that the synthetic apertures of adjacent antennas do not overlap.

In order to correctly predict the eigenvalue spectrum, the aperture length, L_α, used in the analysis must be the sum of the aperture lengths of each antenna. For nonoverlapping apertures in a sidelooking configuration, the total effective aperture is easily calculated as $L_\alpha \approx NM2vT_R$, which is the maximum attainable. If the distance between the first and last effective samples is used, the theoretical curves will be incorrectly scaled in the horizontal dimension.

Another way to consider the distributed case is to consider the block diagonal structure of the CCM. If the data samples taken by adjacent antennas do not overlap, then the correlation between data samples taken on different antennas approaches zero and the CCM becomes block diagonal. Since the eigenvalues of a block diagonal matrix are equal to the eigenvalues of the blocks, we can consider the eigenvalues of each block independently. When there is no Doppler aliasing, then the temporal data samples of each antenna form a uniformly sampled data system with no aliasing of the PSD. Hence, the aperture-bandwidth product applies where the aperture is defined by the effective temporal aperture of the single antenna. Then, the eigenvalues of the temporal covariance matrix for each antenna follow the shape of the PSD, but are scaled in

power by $1/N$. When the eigenvalues from all N antennas are combined, the clutter PSD is fully and accurately represented.

Finally, we mention the case of a distributed array and an illumination bandwidth that exceeds the sample rate defined by the minimum interval between any two effective samples. For the sidelooking distributed array with nonoverlapping synthetic apertures, for example, this minimum interval is $2vT_R$. If the illuminated bandwidth exceeds $1/2vT_R$, then the aperture-bandwidth product exceeds the dimension of the CCM. Hence, the eigenfunctions cease to be well-defined sinusoids and the proposed theory breaks down. In this case, clutter power spans the entire measurement space, making space-time filtering ineffective.

V. Conclusions

One prerequisite for performing moving target indication is that there must be measurement degrees of freedom available after rejection of ground clutter. This requirement means that clutter cannot occupy the entire measurement space, or that the number of significant eigenvalues of the clutter covariance matrix must be less than the matrix's dimension. In other words, clutter rank must be less than the number of measurements.

In traditional space-time processing, clutter rank is held below the number of measurements through the use of periodic time sampling and periodic, Nyquist spatial sampling. Under ideal conditions, this approach leads to a number of unique measurements of clutter that is well below the total number of measurements collected. For arbitrarily-configured arrays, however, current methods of clutter rank prediction do not apply. We feel that the analysis presented in this paper can be useful to the design and analysis of STAP systems employing arbitrary arrays.

In this paper, we have presented a generalized method of estimating clutter rank. This method is based on an equivalent data projection and on the KL representation of a random process. We have presented the theoretical foundation for such an approach to clutter rank, and we have presented simulated examples that span a wide range of array configurations, transmit beamwidths, and look geometries.

References

[1] M. Zatman, "Circular array STAP," *IEEE Trans. Aerosp. Electron. Syst.*, vol. 36, no. 2, pp. 510–517, Apr. 2000.

[2] T. K. Sarkar and R. Adve, "Space-time adaptive processing using circular arrays," *IEEE Antennas Propag. Mag.*, vol. 43, no. 1, pp. 138–143, Feb. 2001.

[3] R. K. Hersey, W. L. Melvin, J. H. McClellan, and E. Culpepper, "Adaptive conformal array radar," in *Proc. 2004 IEEE Radar Conf.*, Philadelphia, PA, pp. 568–572.

[4] J. Ward, "Space-time adaptive processing with sparse antenna arrays," in *Proc. 1998 32nd Asilomar Conf. Signals, Syst., Comp.*, Pacific Grove, CA, pp. 1537–1541.

[5] R. Burns *et al.*, "Techsat 21: formation design, control, and simulation," in *Proc. 2000 IEEE Aerospace Conf.*, Big Sky, MT, pp. 19–25.

[6] L. E. Brennan and F. M. Staudaher, Subclutter Visibility Demonstration Adaptive Sensors Incorporated, Tech. Rep. RL-TR-92-21, Mar. 1992.

[7] J. Ward, Space-Time Adaptive Processing for Airborne Radar MIT Lincoln Laboratory, Lexington, MA, Tech. Rep. 1015, Dec. 1994.

[8] A. Manikas, *Differential Geometry in Array Processing*. London, U.K.: Imperial College Press, 2004.

[9] R. Klemm, *Space-Time Adaptive Processing*. London, U.K.: Institute of Electrical Engineers, 1998.

[10] ——, "Adaptive airborne MTI: an auxiliary channel approach," *Proc. Inst. Electr. Eng.*, vol. 134, no. 3, pt. F, pp. 269–276, Jun. 1987.

[11] ——, "Adaptive clutter suppression for airborne phase array radars," *Proc. Inst. Electr. Eng.*, vol. 130, no. 1, pt. F, pp. 125–132, Feb. 1983.

[12] ——, "Introduction to space-time adaptive processing," *Electron. Commun. Eng. J.*, vol. 11, no. 1, pp. 5–12, Feb. 1999.

[13] K. M. Buckley, "Spatial/spectral filtering with linearly constrained minimum variance beamformers," *IEEE Trans. Acoust., Speech, Signal Process.*, vol. 35, no. 3, pp. 249–266, Mar. 1987.

[14] H. J. Landau and H. O. Pollak, "Prolate spheroidal wave functions, Fourier analysis and uncertainty—III: the dimension of the space of essentially time- and band-limited signals," *Bell Syst. Tech. J.*, vol. 41, pp. 1295–1336, Jul. 1962.

[15] Q. Zhang and W. B. Mikhael, "Estimation of the clutter rank in the case of subarraying for space-time adaptive processing," *Electron. Lett.*, vol. 33, no. 5, pp. 419–420, Feb. 27, 1997.

[16] H. L. Van Trees, *Detection, Estimation, and Modulation Theory, Part I*. New York: Wiley, 1968.

[17] D. Slepian and H. O. Pollak, "Prolate spheroidal wave functions, Fourier analysis and uncertainty—I," *Bell Syst. Tech. J.*, vol. 40, pp. 43–64, Jan. 1961.

Nathan A. Goodman (S'98–M'02) received the B.S., M.S., and Ph.D. degrees in electrical engineering from the University of Kansas, Lawrence, in 1995, 1997, and 2002, respectively.

From 1996 to 1998, he was an RF Systems Engineer for Texas Instruments, Dallas, TX. From 1998 to 2002, he was a Graduate Research Assistant in the Radar Systems and Remote Sensing Laboratory, University of Kansas. He is currently an Assistant Professor in the Department of Electrical and Computer Engineering, University of Arizona, Tucson. Within the department, he directs the Laboratory for Sensor and Array Signal Processing. His research interests are in radar and array signal processing.

Dr. Goodman was awarded the Madison A. and Lila Self Graduate Fellowship from the University of Kansas in 1998. He was also awarded the IEEE 2001 International Geoscience and Remote Sensing Symposium Interactive Session Prize Paper Award.

James M. Stiles (S'91–M'95–SM'97) received the B.S. degree in electrical engineering from the University of Missouri, Columbia, in 1983, the M.S. degree in electrical engineering from Southern Methodist University, Dallas, TX, in 1987, and the Ph.D. degree in electrical engineering from the University of Michigan, Ann Arbor, in 1996.

From 1983 to 1990, he was a Microwave Systems Design Engineer for Texas Instruments, Dallas, TX. From 1990 to 1996, he was a Graduate Research Assistant in the Radiation Laboratory, University of Michigan. Since 1996, he has been an Associate Professor of Electrical Engineering and a member of the Radar Systems and Remote Sensing Laboratory (RSL) at the University of Kansas, Lawrence. His research interests include radar remote sensing of vegetation, propagation and scattering in random media, ground-penetrating radar, and radar signal processing.